Global Stability and Flow Transition in Horizontal Convection

Pierre-Yves Passaggia, Albeto Scotti and Brian White

Department of Marine Sciences,
University of North Carolina, Chapel Hill, NC 27599, USA
passaggia@unc.edu

Abstract

Horizontal convection is considered as a simple model to study the influence of heating and cooling at the ocean surface on the Meridional Overturning Circulation. We outline recent work on the global stability of horizontal convection and its influence on flow transition and the onset of turbulence with increasing Rayleigh number. The transition to turbulence is investigated using a combination of continuation procedure, stability analyses and DNS. Past a critical value for Ra, the base flow becomes unstable first to three-dimensional perturbations and at higher still Ra to two-dimensional instability. At higher Ra, the mechanisms responsible for transition to turbulence are presented using a bifurcation analysis. At $Ra = 2.6 \times 10^7$, the flow exhibits a sub-critical bifurcation which substantially modifies the circulation. The results of companion DNS confirm this scenario leading to a retroflection of the plume. full plume reflection is observed at $Ra \approx 10^{12}$, and the bottom of the domain progressively fills with stagnant heavy fluid, a process which likely explains the shutdown of the core circulation first hypothesized by Sandström (1908).

1 Introduction

Circulations driven by a differential buoyancy forcing applied along a horizontal surface describe for example the atmosphere of Venus which absorbs most of the incoming solar radiation along its upper edge (Houghton, 1977). The world's ocean Meridional Overturning Circulation is subject to a similar forcing where differential heating is imposed between the pole and the equator. Flows driven by this type of boundary conditions are called Horizontal Convection (HC) (Stern, 1975).
HC flows are characterized by three nondimensional parameters: The aspect ratio of the domain $A = L_x/L_z$, the Prandtl number $\mathrm{Pr} = \nu/\kappa$ which quantifies the ratio of viscosity to diffusivity of the stratifying agent and the Rayleigh number $Ra \equiv \delta b H^3/\nu\kappa$, which measures the relative strength of the buoyancy forcing relative to viscous forces. Here we essentially focus our attention on the effect of the Rayleigh number. Unlike the much more studied Rayleigh-Bénard convection, HC has attracted much less attention. The pioneering experimental work of Sandström (1908) led to the hypothesis that an asymptotic regime existing at high values of the Rayleigh number characterized by a shallow surface circulation. Jeffreys (1925) later argued that for a surface-forced flow, the thermodynamics requires only that the return flow of the dense fluid has to occur underneath the flow of light fluid. A rigorous bound was developed by Paparella and Young (2002) on the amount of kinetic energy dissipation that occurs within a horizontally convecting flow. This result, is known as the "anti-turbulence" theorem and questions whether HC can sustain a deep overturning turbulent circulation at high values of the Rayleigh numbers. Whether a truly turbulent flow exists in HC has been the object of several studies (Scotti and White, 2011; Stewart et al., 2011; Griffiths et al., 2013; Gayen et al., 2013), which together show that for values of the Rayleigh number greater than a critical value, HC

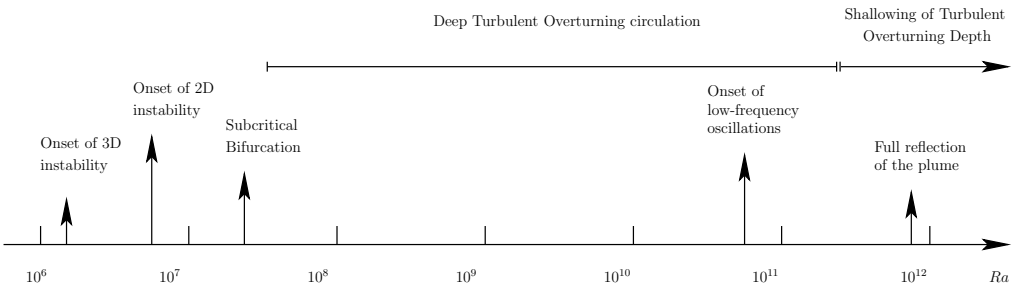

Figure 1: Sketch of the different transitions of horizontal convection in a rectangular cavity, using a step function for the buoyancy imposed at the surface and free slip boundary conditions.

flows for various values of the Prandtl number are characterized by a deep overturning turbulent flow, characterized by a mixing efficiency near unity.
In the present work, we present the successive transition mechanisms leading to turbulence responsible for the confinement of the circulation under the surface for large values of the Rayleigh number. The successive instability mechanisms are summarized in figure 1 where the present work was performed at a Prandtl number equal to unity and an aspect ratio $A = 4$. The boundary condition at the surface is a step function where the cooling side is defined by $x < 0$, $b = 1$ and the warming side is given by $x > 0$, $b = 1$. The rest of the domain is insulated and slip boundary conditions are imposed on all the boundaries.

2 Global Instability Analysis

The basic flow generates an unstable density profile in the surface cooling layer, which approaches the plume region as a narrow jet (c.f. figure 3(,b)). This narrow jet near the left boundary sinks as a sinking plume that reaches and fills the bottom of the domain. The flow progressively diffuses in a broad upwelling region that reaches a strongly stratified layer under the warming boundary.

In the cooling layer, the fluid is subject to the destabilizing effect of cooling at the top and shear within the jet. As a result, this gravitationally unstable region is expected to excite Rayleigh-Taylor (R-T) type instabilities.

In the present low-Rayleigh number regime, the flow characteristics follow the Rossby scaling $\mathrm{Ra}^{1/5}$ (Rossby, 1965). Thus for increasing values of Ra, the boundary layer thickness slowly decreases and diffusion cannot smooth out the unstable density contrast and the R-T instability is expected to become active. In the following sections, we show that the flow is subject to two different types of instabilities. The steady flow initially becomes unstable with respect to a three-dimensional instability, which is characterized by transverse counter-rotating rolls localized in the plume region, defined by the wavenumber β associated with the direction y. The second instability, sets in at a higher Ra, is two-dimensional and is associated with a sheared Rayleigh-Taylor instability located in the thin jet under the cooling layer.

In the remaining of the present section, steady solutions and the associated global stability results were obtained across the range $8.\,10^5 \leq Ra \leq 2.\,10^8$. The choice was made to use a time stepper approach to compute both the steady states and the eigenvalue problem associated with the stability. The same procedure was used in Passaggia et al. (2014) and details about the numerical methods can be found in Marquillie and Ehrenstein

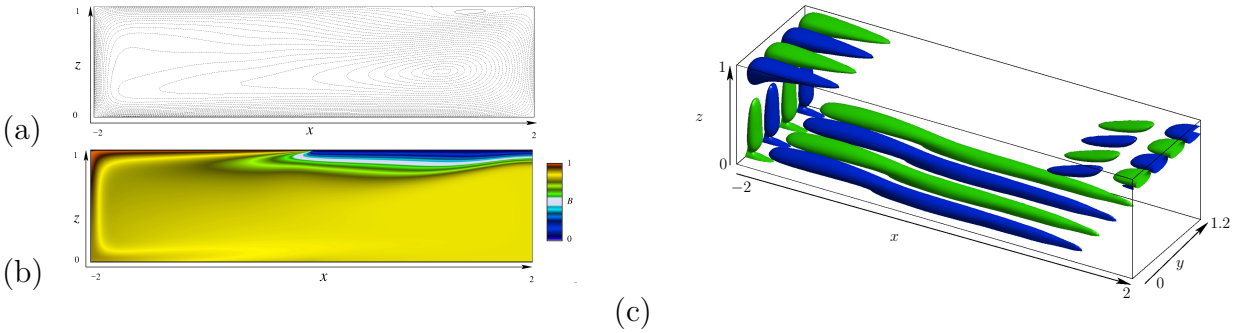

Figure 2: Streamlines (a) and buoyancy distribution (b) of the steady base flow at Ra $= 2.\,10^6$. Visualization of the three-dimensional unstable eigenmode by mean of iso-buoyancy surfaces $\hat{b} = \pm 10\%$ normalized by the maximum of $\hat{b}$ (green/blue) at Ra $= 2.26\,10^6$, Pr $= 1$, $\beta = 10.5$. The width of the box is $0 \leq y \leq 1.2$.

(2002). Equilibrium-states, steady solutions of the Navier-Stokes system are computed using the selective frequency damping method (Akervik et al., 2006). The eigenvalue problem is computed using a time-stepper approach following the algorithm in Edwards et al. (1994)

2.1 Onset of Instability: Steady Three-Dimensional modes

For sufficiently small Rayleigh numbers, the two-dimensional flow solution is stable. The problem is thus marched in time to converge to a steady state which is achieved at $t \approx 1000$. For instance, at $Ra = 2.\,10^6$ the flow is characterized by a single counterclockwise rotating cell spanning the entire domain, and a small clockwise rotating cell, located under light layer of fluid, near the surface in the top right corner (cf. figure 2(a,b)).

The recent DNS results of Gayen et al. (2014) show that the first instability is three dimensional and is characterized by steady counter-rotating vortices with axes aligned along the x direction. The eigenvalue problem is solved for the baseflow shown in figures 2(a,b) and a family of unstable $3D$ steady modes is found (see figure 2c). These modes have been observed for a large range of Rayleigh numbers and mark the onset of instability in horizontal convection. To study these modes, global stability analyses have been performed over a range of Rayleigh numbers $Ra = [1.8\,10^6, 2.26\,10^6]$, transverse wave numbers $\beta = [9, 13]$ where growth rates in the range $\omega_i = [-3.2\,10^{-3}, 4.45\,10^{-3}]$ are found. Increasing the Rayleigh number appears to increase both the growth rate and the most unstable wavenumber, as well as the unstable wave number range. The critical Rayleigh number for this mode was found at $Ra_{c,3D} \sim 1.94\,10^6$ and gives the onset of instability for the present geometry.

2.2 Unsteady Mixing: Two-dimensional Instability

Increasing further the Rayleigh number, the simulation progressively more unstable and the selective frequency damping method was coupled starting at $Ra = 5.\,10^7$ to allow convergence to a steady state. Increasing the Rayleigh number also increases the complexity of the flow and the main recirculation cell exhibits a complex structure with co-rotating vortices, essentially located in the lower part of the domain, under the warm fluid layer (see figures 3(a,b) at $Ra = 2.57\,10^7$).

The critical value for the onset of the two-dimensional instability ($\beta = 0$) is found to be $Ra_{c,2D} \sim 8.05\,10^6$. The structure of the mode mostly spans the left and the bottom boundaries of the flow and takes the form of regular transverse vortices shed along the

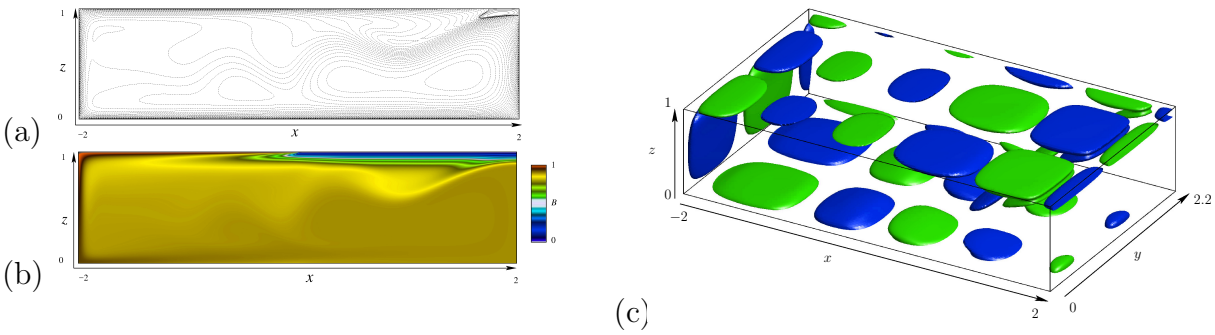

Figure 3: Streamlines (a) and buoyancy distribution (b) of the steady base flow at Ra $= 2.59\,10^7$. Visualization of the three-dimensional unstable eigenmodes by mean of iso-buoyancy surfaces $\hat{b} = \pm 10\%$ normalized by the maximum of $\hat{b}$ (green/blue), at Ra $= 2.59\,10^7$, $\beta = 3$. The width of the box is $0 \le y \le 2\pi/3$.

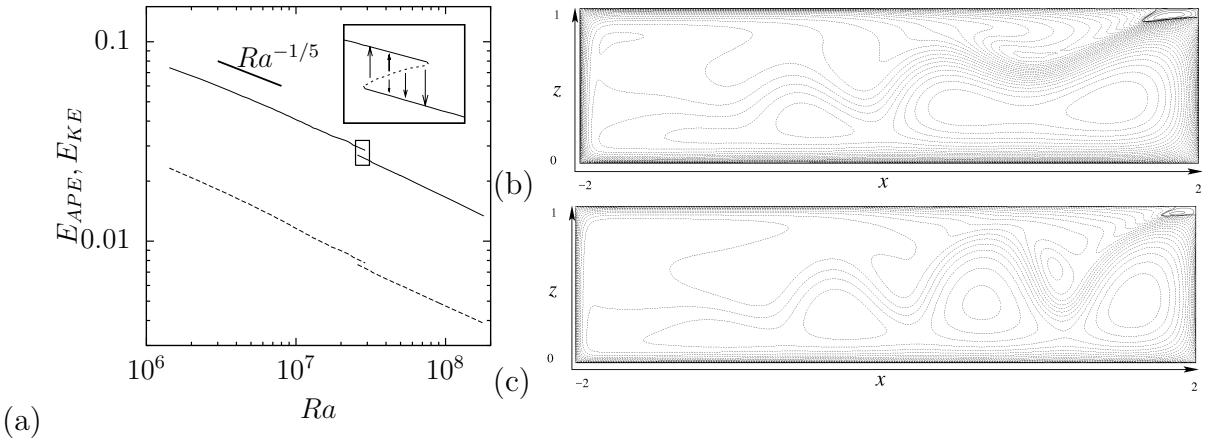

Figure 4: Isovalues of the stream function $\psi(x, z)$ for the two-dimensional steady baseflow (a) at $Ra = 2.59\ 10^7$ for the upper branch (a) and the lower branch (b), Pr $= 1$ (arbitrary scale). The continuous lines show a clear reduction of the recirculation region on the top right corner (clockwise rotation) whereas the dotted lines show the change of pattern in the deep circulation characterized by steady rolls (counter-clockwise rotation). Evolution of the APE (——) and KE (- - -) (c) for the steady states as a function of Ra. The scalings $Ra^{-1/5}$ is compared also against the energetics of the baseflow.

base of the domain, which effectively transport kinetic and potential energy near the boundaries of the domain. While instability is essentially $2D$, similar modes are found in the global spectrum for small β corresponding to wavelengths larger than the depth of the domain. For instance, figure 3c shows the most unstable $2D$ type eigenfunction for $\beta = 3$ at $Ra = 2.57\,10^7$

3 Sub-Critical Bifurcation of the Baseflow

The energy diagnosis in Boussinesq stratified flows relies on the evaluation of kinetic energy (KE) and available potential energy (APE). While the local kinetic energy density is $E_{KE}(\mathbf{x}) = \frac{1}{2}(U^2(\mathbf{x}) + W^2(\mathbf{x}))$, we use for the local definition (Scotti and White, 2014) for the available potential energy

$$E_{APE}(\mathbf{x}) = \int_{b_*(\mathbf{x})}^{b(\mathbf{x})} (z - z_*(s))\, \mathrm{d}s$$

where $z_*(s)$ is the reference height and $b_*(z)$ the reference profile implicitly defined by the relationship $z_*(b_*(z)) = z$. The resorted buoyancy field $b_*(z)$ is defined by the minimum energy state of the system. This profile is a monotonically decreasing profile consisting of

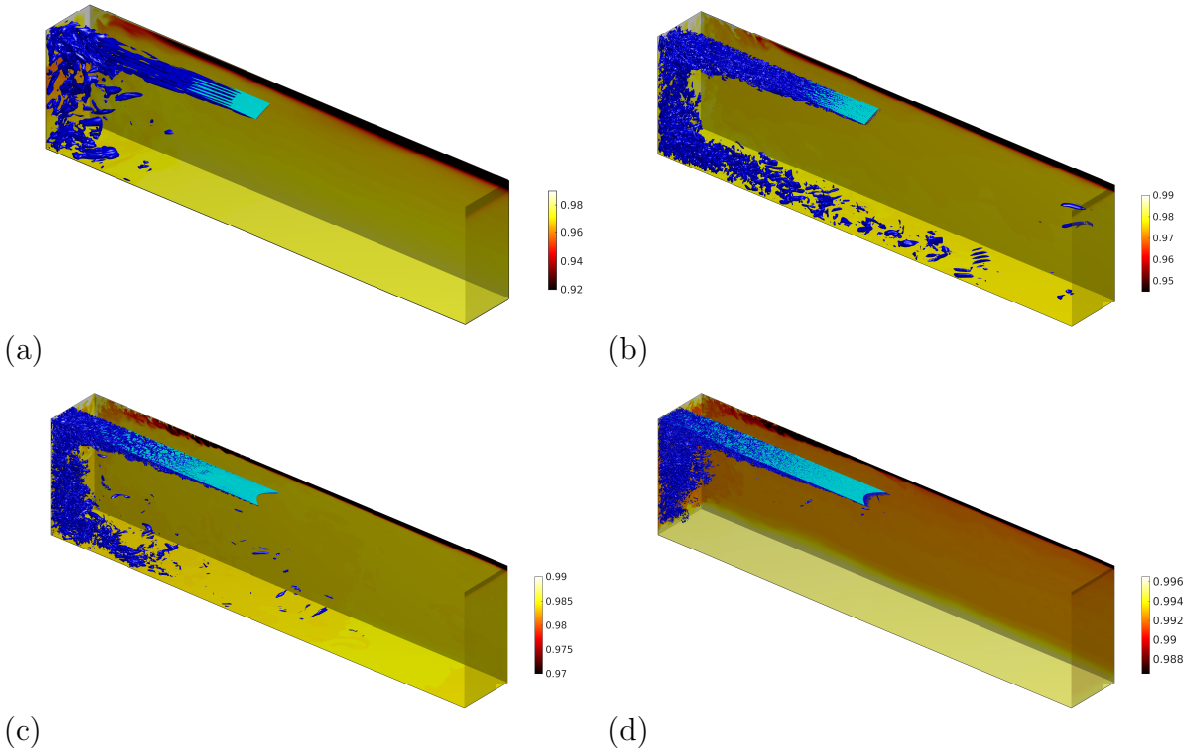

Figure 5: Snapshot of a buoyancy field b (background), the associated $\lambda_2 = -0.1$ criterion (Jeong and Hussain, 1995) (blue iso-contours). The most active regions of vertical gradient of buoyancy $(\partial b)/(\partial z) = 2.\,10^3 Ra^{1/5}$ are also shown (cyan iso-contours) to represent the transition from the transitional regime at $Ra = 10^9$ (a) and turbulent regimes at $Ra = 10^{10}$ (b), $Ra = 10^{11}$ (c) and $Ra = 10^{12}$ (d) where the plume reflection is visible. Note the different color scale for buoyancy showing the heavy layer of fluid sitting at the bottom for $Ra = 10^{12}$ (d).

the isochoric resorting of the heavier particles of fluid at the bottom and the lighter ones at the top.

The first equilibrium state obtained using an Recursive Projection Method (RPM) based arc-length continuation procedure (Shroff and Keller, 1993) initialized at $Ra = 1.42\,10^6$ shows that the two-dimensional base flow is globally stable. The continuation procedure was computed until $2.89\,10^7$ where the algorithm diverges. Restarting the RPM procedure at $3.\,10^7$ and computing solutions backward in Ra until $2.48\,10^7$, two steady solutions are found to coexist over a small Ra region (see figure 4a). This transition is characterized by a change of behavior of the flow inside the domain shown in figure 4 (b,c). For increasing values of Ra the flow bifurcates from two to four steady rolls in the interior of the domain. This bifurcation is responsible for an important decrease of KE and APE.

Transition from one branch of solution to an other at constant Ra can be achieved by a finite amplitude perturbation. Using a combination between the upper branch and the lower branch solution and evolving this field as an initial condition for the simulation, the flow is found to evolve on either one branch of the other. This is illustrated in figure 3a where the dashed line in the close up view shows the the branch towards which the solution evolves and highlights the sub-critical nature of the bifurcation. Gayen et al. (2014) reported the existence of a jump in the Nusselt number in their DNS for Ra $\approx 510^7$ for somewhat different boundary conditions and values of Pr. These results show that the present bifurcation is a robust feature that drives the onset of plume reflection.

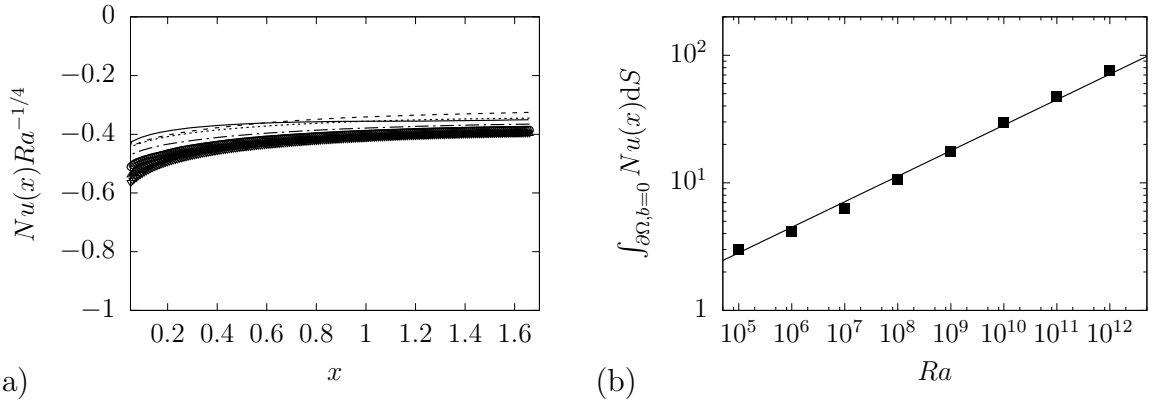

Figure 6: Nusselt number along the longitudinal coordinate x at the surface ($z = H$), in the unstable region ($b = 1$) rescaled with the viscous scaling $\mathrm{Ra}^{-1/5}$ (a), in the stable region ($b = 1$) (a). The solid lines represent the laminar/unsteady solutions ($10^6 \leq \mathrm{Ra} \leq 10^8$), whereas the symbols are for the turbulent solutions ($10^9 \leq \mathrm{Ra} \leq 10^{12}$). Nusselt vs. Rayleigh number (■) where the solid line is the scaling $\mathrm{Ra}^{1/5}$ (b).

4 Turbulent Direct Numerical Simulations

The Navier-Stokes equations are solved numerically using a standard DNS code (see Scotti and White, 2011, and references therein for details) and figure 5 shows snapshots of the field for different values of the Rayleigh number. For values of Ra up to 10^{11}, The flow is found to sustain a turbulent deep overturning circulation. However at $\mathrm{Ra} \approx 10^{12}$ the turbulent descending plume does not reach the bottom anymore. Instead the bottom is filled with heavy stagnant fluid 5 and turbulence appears to be progressively confined under the surface.

The question hence arises weather the $Ra^{1/5}$ Rossby scaling is found to change, at least for the higher value of the Rayleigh number. Such question was addressed recently by Shishkina et al. (2016) where the exponent was conjectured to change from 1/5 to 1/4 when the flow becomes fully turbulent. There assumption relies on the fact that boundary layer under the cooling layer becomes unstable. The nusselt number, wihch in our units writes

$$\mathrm{Nu} = \left.\frac{\partial \mathrm{b}}{\partial \mathrm{z}}\right|_{\mathrm{b=Cst.}}$$

measured along the warm layer $b(x > 0, z = 1)$, is shown as a function of the Rayleigh number in figure 6(a,b). Despite the flow being fully turbulent under the unstable layer and the full plume reflection regime, the scaling follows the 1/5 scaling. This is a consequence of the flow remaining laminar in the stratified region located under wram layer of fluid and acting as a buffer zone for both turbulence and heat exchanges.

In order to better understand if the warming/stratfied layer can become turbulent, we derive a lower bound on the Richardson number. The simulations show that in the warm boundary layer the buoyancy field depends, to first approximation, only on the vertical coordinate z. The flow consists mostly of an horizontally uniform upwelling, which is well approximated by an inviscid corner flow. In the buoyancy equation the balance is between vertical upwelling and diffusion (recall that in our inviscid units $\kappa = (\mathrm{PrRa})^{-1/2}$)

$$wb - (\mathrm{PrRa})^{-1/2}\frac{\partial \mathrm{b}}{\partial \mathrm{z}} = \mathrm{O}\left(\mathrm{Nu}(\mathrm{PrRa})^{-1/2}\right), \tag{1}$$

where Nu is the Nusselt number. Following Rossby (1998), we assume that a single length scale δ describes both the kinetic and the buoyancy layer. This is justified if $\mathrm{Pr} = \mathrm{O}(1)$

and the flow remains laminar. It is well verified by the DNS. Note however that the same assumption does not hold in the turbulent region under the cooling section of the boundary. We also introduce a streamfunction Ψ, which locally can be written as

$$\Psi = U\delta x \tag{2}$$

Requiring that all terms in (1) have the same order of magnitude, we have

$$\delta = O(\mathrm{Nu}^{-1}),\ \mathrm{w} = -\frac{\partial \Psi}{\partial \mathrm{x}} = \mathrm{U}\delta = \mathrm{O}(\mathrm{Nu}(\mathrm{PrRa})^{-1/2}). \tag{3}$$

The thinning of the boundary layer causes shear $S \sim U/\delta$ to increase as well, thus potentially leading to a destabilizing effect if the magnitude of the Richardson number decreases below the threshold for Kelvin-Helmholtz instabilities. This however does not occur because of the 1/5 Rossby scaling and the Richardson number

$$\mathrm{Ri} \equiv \frac{N^2}{S^2} = O\left(\frac{\delta}{U^2}\right) = O(\mathrm{PrRa}^{-1/5}), \tag{4}$$

does not decrease at high Ra, indeed it remains above the threshold for instability across the range of Rayleigh numbers considered in this study. Furthermore, it also shows that increasing Pr only further stabilizes this stably stratified region. This result shows that for $\mathrm{Pr} \geq 1$, HC is unlikely to become fully turbulent and follows the early inituition of Sandström (1908).

5 Conclusions

We report the scenario leading to transition to turbulence in Horizontal Convection using a global stability analysis, a bifurcation analysis and turbulent direct numerical simulations. The flow is found to become unstable prior to three and two-dimensional type instabilities successively, both of Rayleigh-Taylor type. Increasing the value of the Rayleigh number the flow exhibits a sub-critical bifurcation which is reponsible for the onset of plume reflection and also sets the transition to turbulence. The full reflection of the plume is finally observed at $\mathrm{Ra} \approx 10^{12}$ where turbulence remains confined under the cooling boundary. The exponent associated with the heat exchanges of the turbulent dynamics is found to follow the laminar scaling $\mathrm{Nu} \sim \mathrm{Ra}^{1/5}$ of Rossby (1965) for all values of Ra. A lower bound for the Richardson number is also derived and shows that the flow in the warm layer remains laminar for all values of Ra, at least for values of Pr greater than unity. Therefore the turbulent $\mathrm{Nu} \sim \mathrm{Ra}^{1/4}$ scaling recently predicted by Shishkina et al. (2016) may be observed for $\mathrm{Pr} \geq 1$ in turbulent simulations but the region where a turbulent scaling can be observed will be confined to a narrow region of the flow that shrinks as Ra increases since the overall scaling must be of order $\mathcal{O}(\mathrm{Ra}^{1/5})$.

References

Akervik, E., Brandt, L., Henningson, D. S., Hœpffner, J., Marxen, O., and Schlatter, P. (2006). Steady solutions of the Navier-Stokes equations by selective frequency damping. *Phys. of Fluids*, 18(6).

Edwards, W. S., Tuckerman, L. S., Friesner, R. A., and Sorensen, D. C. (1994). Krylov methods for the incompressible navier-stokes equations. *Journal of Computational Physics*, 110(1):82–102.

Gayen, B., Griffiths, R. W., and Hughes, G. O. (2014). Stability transitions and turbulence in horizontal convection. *J. of Fluid Mech.*, 751:698–724.

Gayen, B., Griffiths, R. W., Hughes, G. O., and Saenz, J. A. (2013). Energetics of horizontal convection. *J. of Fluid Mech.*, 716.

Griffiths, R. W., Hughes, G. O., and Gayen, B. (2013). Horizontal convection dynamics: Insights from transient adjustment. *J. of Fluid Mech.*, 726:559–595.

Houghton, J. T. (1977). *The physics of atmospheres*. Cambridge University Press.

Jeffreys, H. (1925). On fluid motions produced by differences of temperature and humidity. *Q. J. R. Meteorol. Soc.*, 51:347–356.

Jeong, J. and Hussain, F. (1995). On the identification of a vortex. *J. of Fluid Mech.*, 285:69–94.

Marquillie, M. and Ehrenstein, U. (2002). Numerical simulation of separating boundary-layer flow. *Computers Fluids*, 31:683–693.

Paparella, F. and Young, W. R. (2002). Horizontal convection is non-turbulent. *J. of Fluid Mech.*, 466:205–214.

Passaggia, P.-Y., Meunier, P., and Le Dizès, S. (2014). Response of a stratified boundary layer on a tilted wall to surface undulations. *J. of Fluid Mech.*, 751:663–684.

Rossby, H. T. (1965). On thermal convection driven by non-uniform heating from below: an experimental study. *Deep-Sea Res.*, 12:9–16.

Rossby, T. (1998). Numerical experiments with a fluid heated non-uniformly from below. *Tellus*, 50A:242–257.

Sandström, J. (1908). Dynamische versuche mit meerwasser. *Ann. Hydrogr. Marit. Meteorol.*, 36:6–23.

Scotti, A. and White, B. (2011). Is Horizontal convection really "non turbulent"? *Geophys. Res. Lett.*, 38:L21609.

Scotti, A. and White, B. W. (2014). Diagnosing mixing in stratified turbulent flows with a locally defined available potential energy. *J. of Fluid Mech.*, 740:114–135.

Shishkina, O. S., Grossman, S., and Lohse, D. (2016). Heat and momentum transport scalings in horizontal convection. *Geophys. Res. Lett.*, 43(3):1219–1225.

Shroff, G. M. and Keller, H. B. (1993). Stabilization of Unstable Procedures: The Recursive Projection Method. *SIAM J. on Numer. Anal.*, 30(4):1099–1120.

Stern, M. (1975). *Ocean Circulation Physics*. New York:Academic.

Stewart, K. D., Hughes, G. O., and Griffiths, R. W. (2011). When do marginal seas and topographic sills modify the ocean density structure? *J. Geophys. Res.*, 116:C08021.